Quasiparticle energies and dielectric functions of diamond polytypes

Masahiro Sakurai,[1,*] James R. Chelikowsky,[1,2,3] Steven G. Louie,[4,5] and Susumu Saito[6]
[1]*Center for Computational Materials, Institute for Computational Engineering and Sciences, The University of Texas at Austin, Austin, Texas 78712, USA*
[2]*Department of Chemical Engineering, The University of Texas at Austin, Austin, Texas 78712, USA*
[3]*Department of Physics, The University of Texas at Austin, Austin, Texas 78712, USA*
[4]*Department of Physics, University of California, Berkeley, California 94720, USA*
[5]*Materials Sciences Division, Lawrence Berkeley National Laboratory, Berkeley, California 94720, USA*
[6]*Department of Physics, Tokyo Institute of Technology, Meguro, Tokyo 152-8551, Japan*
(Received 29 August 2017; published 25 October 2017)

We perform *ab initio* many-body Green's function calculations to investigate the quasiparticle energies and optical properties of diamond polytypes that have been predicted to be producible via a pressure-induced structural phase transition from carbon nanotube solids. We find, through quasiparticle band-structure calculations within the GW approximation, that the band gaps of two hexagonal ($2H$- and $4H$-type) polytypes of diamond differ significantly from that of cubic diamond as well as from that of the crystalline sp^3 carbon phase with a body-centered-tetragonal structure, called bct C_4. We also examine the dielectric functions of three polytypes of diamond (cubic, $2H$, and $4H$) by employing the GW plus Bethe-Salpeter equation approach. The calculated optical absorption spectra are found to be distinct from each other. The lattice mismatches of carbon layers of these diamond polytypes are very small and the total-energy differences are also small. Our work opens up the possibility of fabricating diamond superlattices with various electronic and optoelectronic properties by utilizing and controlling the different stacking sequences of carbon layers.

DOI: 10.1103/PhysRevMaterials.1.054603

I. INTRODUCTION

Face-centered-cubic (fcc) and hexagonal-close-packed (hcp) structures both have a close-packed arrangement of atoms. The difference between the fcc and hcp structures is the stacking sequence of close-packed atomic layers along the stacking axis. The period of other stacking sequences is known to be longer in certain materials. The best known example is silicon carbide (SiC) [1]. The crystal structure of an SiC polytype can be specified by its stacking pattern. For example, a hexagonal SiC polytype, called nH-SiC, repeats its stacking sequence with a periodicity of n, forming a hexagonal unit cell. Similarly, an SiC polytype with a zinc-blende structure is referred to as $3C$-SiC, since it possesses a cubic crystalline lattice and has an ABC stacking along its [111] direction. Owing to the difference in the crystal lattice structure, SiC polytypes exhibit a wide variety of electronic and optical properties, which are not only useful to characterize the polytypes but also potentially advantageous for device applications [1]. Because both silicon and carbon atoms have four valence electrons and carbon shows a greater flexibility in its covalent bonding than silicon, a tetrahedrally bonded carbon solid is expected to show polytypism similar to SiC. Indeed, an sp^3-bonded carbon phase with an ABC stacking is nothing but cubic diamond, which exists in nature. The simplest hexagonal counterpart is hexagonal diamond, also named lonsdaleite, which has been suggested to exist in meteorites [2,3] and has also been synthesized by the room-temperature compression of graphite [4]. There is a close equivalence of atomic structures between SiC and diamond polytypes. Thus cubic (hexagonal) diamond can be referred to as $3C$ ($2H$) diamond.

The graphite-to-hexagonal-diamond transition under pressure [4] suggests that other sp^3-bonded carbon phases can be produced by applying high pressure to other sp^2-bonded carbon allotropes, such as fullerene and carbon nanotubes. Shock compression experiments combined with rapid cooling techniques [5,6] have revealed a transformation from a C_{60} fullerene solid into "amorphous diamond," an sp^3-rich phase with no long-range order. Carbon nanotube solids under moderate pressure have recently been predicted to transform into a variety of diamond phases from constant-pressure molecular dynamics (MD) simulations [7–9]. The resultant phases include two hexagonal ($2H$ and $4H$) polytypes of diamond and a fourfold coordinated carbon phase having a body-centered-tetragonal (bct) lattice [10], called bct C_4. These diamond polytypes are found to be stable not only under pressure but also at zero pressure [9]. As SiC polytypes [11,12], hexagonal polytypes of diamond are expected to have distinct electronic and optical properties in comparison to cubic ($3C$) diamond. Such novel properties should be of importance in the future device applications of diamond.

In order to clarify the details of the electronic and optical properties of diamond polytypes, we study the quasiparticle energies and optical properties of two hexagonal polytypes of diamond ($2H$ and $4H$) that have been predicted to be producible through the constant-pressure MD simulations of carbon nanotubes under pressure, and compare them to those of other diamond polytypes. We adopt the GW approximation (GWA) [13–15] to investigate the quasiparticle band structures of $2H$ and $4H$ diamond polytypes. We discuss diamond superlattices as a possible application of diamond polytypes. We also examine the dielectric functions of $2H$ and $4H$ diamond polytypes by solving the Bethe-Salpeter equation (BSE) using the *ab initio* GW band structure [16] to take into

*masahiro@ices.utexas.edu

account the electron-hole interaction, which is crucial to obtain an accurate spectrum.

II. COMPUTATIONAL METHODS

The ground-state total energies, as well as the Kohn-Sham single-particle orbitals and corresponding eigenenergies, are calculated in the framework of the density-functional theory [17] in the local density approximation (LDA) [18] as implemented in the QUANTUM ESPRESSO package [19]. We employ the parametrized Ceperley-Alder-type exchange-correlation functional [20,21], the Troullier-Martins norm-conserving pseudopotentials [22,23], and a plane-wave basis set with a cutoff energy of 60 Ry for all LDA calculations.

Quasiparticle energies are evaluated within a "one-shot" GW approximation [13–15] where the frequency-dependent (Fourier-transformed) electron self-energy Σ is given by a convolution of the one-particle Green's function G and the dynamically screened Coulomb interaction W. The Kohn-Sham orbitals and the corresponding energies are used as the input for constructing the Green's function. The static irreducible polarizability is then calculated within the random phase approximation not with the Hartree G but with the LDA G constructed in the aforementioned way. To compute the screened Coulomb interaction, the inverse of the static dielectric matrix derived from the static irreducible polarizability is extended to finite frequencies using the generalized plasmon-pole model [14,15] as implemented in the BERKELEYGW code [24]. The GW approximation gives highly accurate quasiparticle energies and therefore the band-gap energies in comparison to the LDA results. The GW method has been applied to a wide range of semiconductors and insulators [25].

To investigate the optical properties, we adopt the GW plus BSE approach [16,26] which is also implemented in the BERKELEYGW code [24]. The imaginary part of the macroscopic dielectric function is given by

$$\varepsilon_2(\omega) = \frac{16\pi^2 e^2}{\omega^2} \sum_S |\vec{\lambda} \cdot \langle 0|\vec{v}|S\rangle|^2 \delta(\omega - \Omega_S). \quad (1)$$

Here, $\vec{\lambda}$ is the polarization vector of the light, $\vec{v}$ denotes the velocity operator, and $\langle 0|\vec{v}|S\rangle$ represents the optical transition matrix element from the ground state $|0\rangle$ to the excited state $|S\rangle$ which is given in terms of the quasiparticle free electron-hole pair basis functions by $|S\rangle = \sum_{vc} A^S_{vc}|vc\rangle$. The transition energy Ω_S and the corresponding amplitude A^S_{vc} are the solutions of the following eigenvalue equation,

$$(E_c - E_v)A^S_{vc} + \sum_{v'c'} \langle vc|K^{\rm eh}|v'c'\rangle A^S_{v'c'} = \Omega_S A^S_{vc}, \quad (2)$$

where $K^{\rm eh}$ is the electron-hole interaction kernel and the summation runs over the valence bands (v) and the conduction bands (c). The E_v and E_c are the GW quasiparticle energies of valence and conduction bands, respectively. For notational simplicity, we have suppressed the explicit k dependence of all the quantities in Eq. (2). For crystals, it is essential to evaluate the $K^{\rm eh}$ on a very fine k-point grid, which is a computationally demanding task. Here, we use the interpolation scheme proposed by Rohlfing and Louie [16] that aims to capture not only the energy dependence but also the k-point dependence of the self-energy correction. In this scheme, we first calculate the quasiparticle energies and the matrix elements of the kernel on a coarse k-point grid, and then interpolate them onto a dense k-point grid using the tetrahedron method and a wave-function-based interpolation. This interpolation scheme greatly reduces the computational cost without losing accuracy [16]. Once the imaginary part $\varepsilon_2(\omega)$ is obtained, the corresponding real part $\varepsilon_1(\omega)$ is calculated by using a Kramers-Kronig transformation.

III. RESULTS AND DISCUSSION

A. Quasiparticle band structure

We commence with a quasiparticle energy calculation for cubic diamond. The lattice constant is set to be the experimental one, 3.57 Å. The static dielectric matrix is computed with a cutoff energy of 10 Ry. The self-energy is computed with a summation over 20 k points in the irreducible Brillouin zone. The Coulomb-hole contribution to the self-energy converges slowly with respect to the number of empty states included in the calculation [27]. To ensure convergence, we use 300 bands consisting of four valence and the lowest 296 conduction bands. Within the GW approximation, we obtain a fundamental gap of 5.37 eV and a direct gap of 7.13 eV at the Γ point. These results agree well with the experimental values, 5.48 and 7.3 eV, respectively, and are also consistent with the previous GW calculations [14,15].

The lattice constants of $2H$ and $4H$ diamond polytypes are determined by the LDA calculations: $a = 2.475$ Å, $c = 4.127$ Å for $2H$ diamond, and $a = 2.482$ Å, $c = 8.189$ Å for $4H$ diamond. The values obtained for $2H$ diamond agree with the experimental data [2,3] ($a = 2.52$ Å and $c = 4.12$ Å) as well as the theoretical results [28–30]. Our LDA results for $4H$ diamond are also consistent with the previous LDA calculations [30,31]. The calculated LDA total energies of $2H$ and $4H$ diamond polytypes are only 0.024 and 0.010 eV/atom higher than that of cubic diamond, respectively. Unlike cubic diamond, all the carbon-carbon (C-C) bonds are no longer equivalent in $2H$ diamond, where the C-C bond length along the c axis (1.548 Å) is longer than the other ones (1.519 Å). The latter is shorter than the C-C bond in cubic diamond (1.526 Å within the LDA and 1.54 Å in experiment). Similarly, $4H$ diamond has longer C-C bonds (1.535 Å) along the c axis and shorter ones (1.522 Å). With the LDA-optimized geometries, the GW calculations are then performed using a dielectric energy cutoff of 10 Ry, 39 k points, and 400 (800) bands for $2H$ ($4H$) diamond.

Figure 1(a) shows the electronic band structure of $2H$ diamond obtained with the LDA and the GWA. The $2H$ diamond is predicted to be an indirect-gap semiconductor with a band gap of 4.58 eV, which is much smaller than that of cubic diamond (5.37 eV within the GWA) but is significantly larger than that of bct C_4 (3.78 eV within the GWA [10]). The reduction of the band gap is due to the presence of a dispersive conduction band with a minimum at the K point. This state shows a parabolic dispersion around the K point and has a "floating" character [32]. Here, "floating" means that the wave function localizes in interstitial regions rather than atomic or bond sites. Similarly, the interlayer (or surface) state in graphite [33,34] and the nearly-free-electron (NFE)

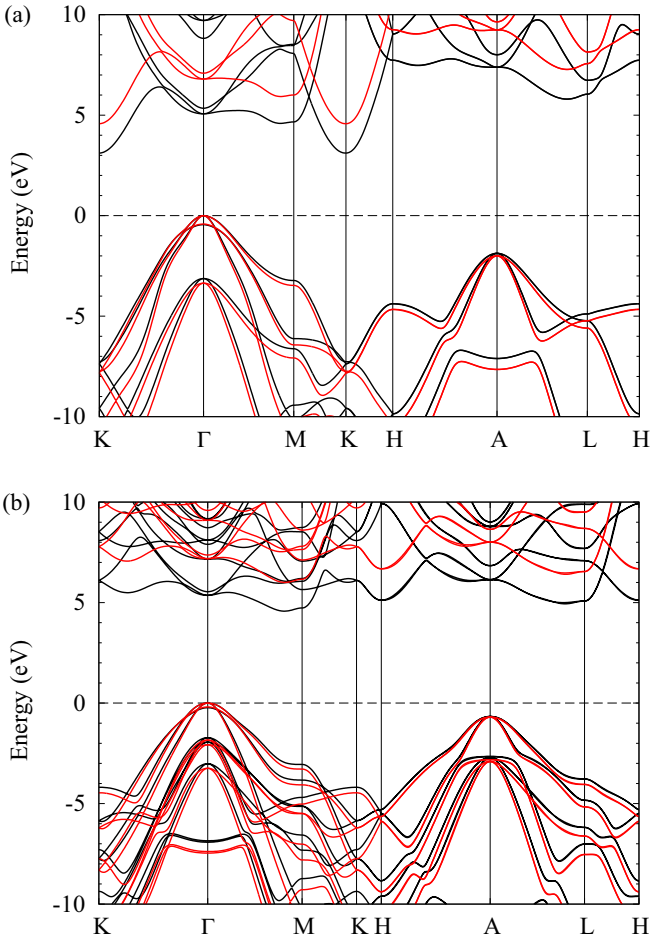

FIG. 1. Electronic band structures of (a) hexagonal ($2H$) diamond and (b) $4H$ diamond, calculated with the LDA (black) and the GWA (red). Energy is measured from the top of the valence band.

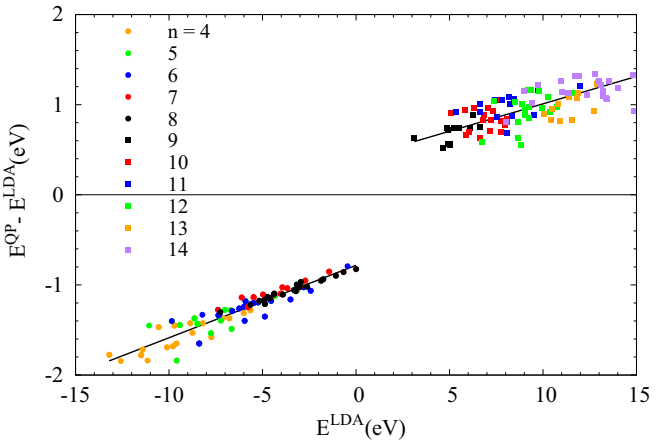

FIG. 2. The GW self-energy correction, that is the difference between the quasiparticle energy $E^{\mathrm{QP}}_{n,k}$ and the LDA energy $E^{\mathrm{LDA}}_{n,k}$, in hexagonal ($2H$) diamond. The data are plotted as a function of the LDA eigenvalue for the five highest occupied and the six lowest unoccupied states ($n = 4$–14) at 39 k points including several high-symmetry points. Energy reference for $E^{\mathrm{LDA}}_{n,k}$ is the top of the valence band. The solid lines, fitted to the data, indicate weak linear dependence.

state in carbon nanotubes [35,36] have wave functions that are also distributed away from atomic sites. The many-body correction within the GWA depresses the NFE state relative to the Fermi level in carbon nanotubes and graphene [37], while the conduction bands around the Fermi level in $2H$ diamond, including the state with a "floating" character, are raised up in energy due to the self-energy correction, as can be seen in Fig. 1(a). This observation is evident in Fig. 2, where the difference between the quasiparticle energy E^{QP} and the LDA one E^{LDA} are plotted. The GW self-energy corrections to the LDA eigenvalues are positive (negative) for all the low-lying conduction (valence) bands. The difference in the GW correction arises from differences in the spatial extent of and the strength of electronic screening to each electronic state. In graphene and carbon nanotubes, the NFE states are much more delocalized than the bonding and antibonding states, and they are located in the vacuum region, a few angstroms away from the carbon plane. Due to these two factors, the self-energy correction to an NFE state is smaller. In diamond, the state having a floating character is in the interstitial region and hence has a larger self-energy correction. Although the GW self-energy corrections for both occupied states and unoccupied states show a weak linear dependence on the LDA eigenvalue, not only their energy but also k-point dependences are of crucial importance in computing the absorption spectrum, which requires the quasiparticle energies at a given k point on a fine grid.

Figure 1(b) shows the electronic band structure of $4H$ diamond calculated by the LDA and the GWA. The quasiparticle band gap of $4H$ diamond is predicted to be 6.00 eV, which is, in contrast to $2H$ diamond, significantly larger than that of cubic diamond as well as that of bct C_4. The hexagonal unit cell of $4H$ diamond is approximately twice longer than that of $2H$ diamond in the direction of the c axis. As a result, a minimum of the low-lying conduction band with parabolic dispersion occurs at the H point. The conduction bands around the K point are moved away from the Fermi level. The absolute bottom of the conduction band is located between the Γ and M points. The direct band gap at the Γ point of $4H$ diamond (7.19 eV within the GWA) is comparable to that of cubic diamond (7.13 eV within the GWA and 7.3 eV in the measurement [38]) and is larger than that of $2H$ diamond (6.80 eV within the GWA). As is the case for $2H$ diamond, the GW self-energy corrections obtained for $4H$ diamond show a weak linear dependence on the LDA eigenvalue, pushing the valence (conduction) bands to lower (higher) energies.

Diamond polytypes with different band gaps and similar lattice constants are promising as a building block for a diamond superlattice. In their first synthesis of diamond superlattice using a different concept [39], Watanabe and co-workers controlled the isotope composition of carbon layers and achieved a band-gap difference of 17 meV to confine the electrons. The band-gap difference in the diamond polytypes, revealed in the present GW study, is much larger than the value measured for isotope-controlled diamond superlattices, making it easier to control carrier confinement. Similar lattice constants of diamond polytypes are also favorable to superlattice structures: (i) Cubic diamond involves an ABC stacking of carbon layers along the [111] direction. This direction is suited

for c-axis-oriented growth of either hexagonal ($2H$) diamond or $4H$ diamond polytypes. In both cases, the lattice-constant mismatch is less than a few percent. (ii) A combination of $2H$ and $4H$ diamond polytypes is highly promising for a superlattice structure. The difference between the LDA lattice constants of carbon layers of these two polytypes is less than 1%. It is expected that one can create multilayer structures consisting of $2H$ and $4H$ diamond polytypes by controlling the stacking sequence along the c axis. (iii) In addition to these diamond polytypes, bct C_4 is another potential candidate. The material consists of AB-stacked carbon layers along the a (or b) axis in the bct unit cell. Its in-plane lattice constant (2.483 Å within the LDA [10]) is approximate to those of $2H$ and $4H$ diamond (2.475 and 2.482 Å, respectively, within the LDA), offering a possibility to combine bct C_4 with either $2H$ or $4H$ diamond polytypes. We note that bct C_4 is predicted to be accompanied by hexagonal diamond in constant-pressure MD simulations of transforming (10,10) carbon nanotube solids under pressure [7].

Diamond is well known to exhibit significant band-gap renormalization due to strong electron-phonon interactions [40,41]. The diamond polytypes that we study here have similar carbon-carbon bond lengths and are expected to have a similar degree of electron-phonon coupling, resulting in a similar band-gap renormalization. The difference in the electron-phonon band-gap renormalization is expected to be smaller than the band-gap difference that we predicted for different diamond polytypes. As shown in the literature, the incorporation of the electron-phonon interaction is necessary to obtain accurately the temperature dependence of the band gap.

B. Dielectric functions and optical properties

We focus on cubic diamond to confirm the reliability of the present GW plus BSE calculation. The quasiparticle energies and the matrix elements of the electron-hole interaction kernel are computed on a coarse 7^3 k-point grid, and we then interpolate them onto a fine 19^3 grid. To achieve a k-point sampling dense enough to evaluate accurately the electron-hole interaction kernel, the fine 19^3 grid is shifted so that the grid contains 6859 crystallographically different k points. In solving the BSE, we include the three highest valence and the four lowest conduction bands.

In Fig. 3, we plot the dielectric functions calculated for cubic diamond. As seen in previous work [16,26], inclusion of the electron-hole interaction changes the amplitude of the entire spectrum, causing a shift of the dominant features of the spectrum to lower energy. The calculated spectra that include the electron-hole interaction are in very good agreement with the experimental data in a wide range of energy. We note that our spectrum does not exhibit a jagged "ghost" structure that has been found in previous calculations [42,43], indicating that a fine enough k-point sampling is realized in our calculation. As shown in Fig. 3(a), the BSE spectrum describes the characteristic features of $\varepsilon_1(\omega)$ quantitatively: a steep, negative slope around 12 eV and a pronounced minimum at about 12.5 eV. The low-energy limit of $\varepsilon_1(\omega)$ gives the high-frequency dielectric constant. The BSE method yields $\varepsilon_\infty = 5.59$, which agrees with the experimental value ($\varepsilon_\infty = 5.7$) [44]. As seen in Fig. 3(b), the position of the absorption

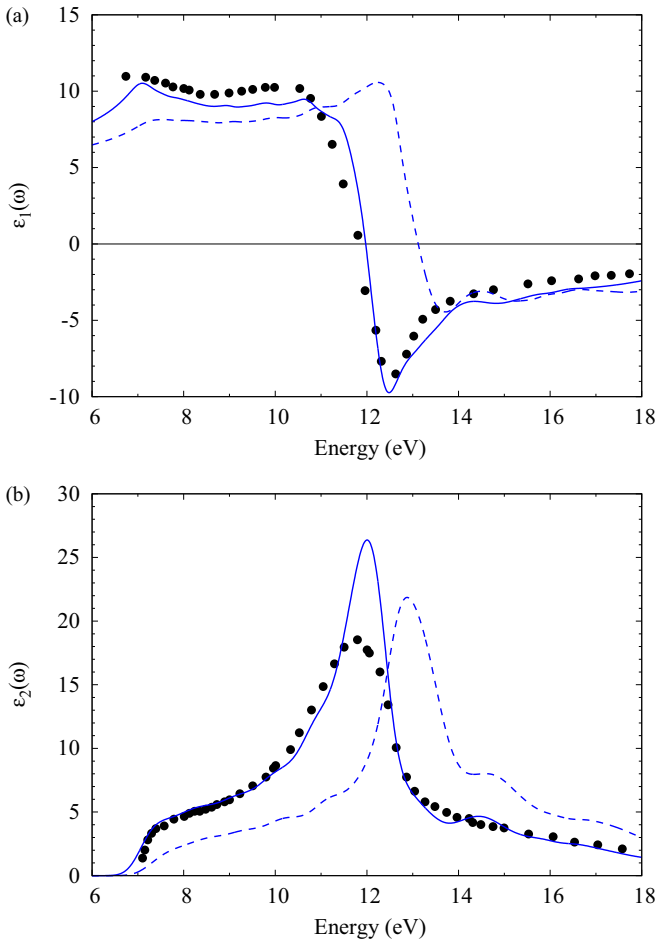

FIG. 3. (a) Real part $\varepsilon_1(\omega)$ and (b) imaginary part $\varepsilon_2(\omega)$ of the macroscopic dielectric function of cubic diamond, calculated with (solid curve) and without (dashed curve) the electron-hole interaction. The calculated spectra (which include a Gaussian broadening of 0.25 eV) are compared to the experimental data (dots) taken from Ref. [45].

maximum agrees well with the experiment, although the BSE spectrum has a larger amplitude around 12 eV than the experiment. Such an overestimation of the spectral weight has also been reported in previous calculations [42,43].

In a similar way to cubic diamond, we apply the BSE method to the $2H$ and $4H$ polytypes of diamond. A coarse k-point grid of $6 \times 6 \times 4$ is used for calculating the quasiparticle energies and the electron-hole kernel before they are interpolated onto a fine k-point grid. In solving the BSE for $2H$ ($4H$) diamond, we use a shifted fine grid of $15 \times 15 \times 10$ ($15 \times 15 \times 6$) and include the five (eight) highest valence and the six (ten) lowest conduction bands. Since the dielectric response of an uniaxial semiconductor shows strong differences for the electric vector parallel to the different principal axis, we consider two directions for the polarization of the light ($\vec{\lambda}$): the one perpendicular to the c axis of the hexagonal unit cell, which gives the ordinary spectrum, and the other parallel to the c axis, which yields the extraordinary spectrum [45].

The imaginary part of the macroscopic dielectric function (which is related to the optical absorption spectrum) for

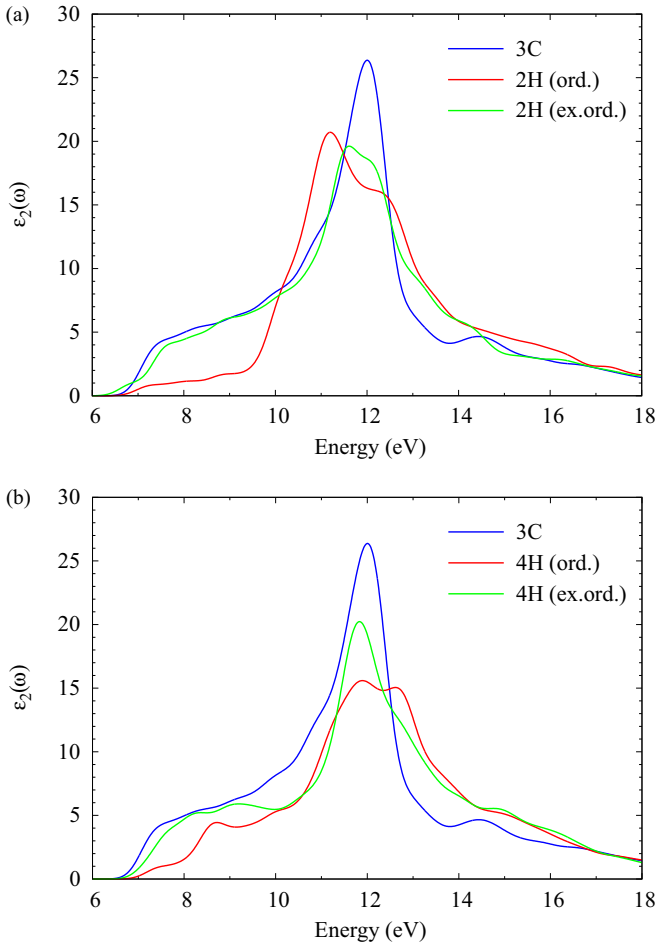

FIG. 4. Imaginary part of the dielectric function $\varepsilon_2(\omega)$ for (a) hexagonal ($2H$) diamond and (b) $4H$ diamond that takes into account the electron-hole interaction. The red (green) curve denotes the ordinary (extraordinary) spectra calculated for the polarization of light perpendicular (parallel) to the c axis. The calculated spectra include a Gaussian broadening of 0.25 eV and are compared to that of cubic ($3C$) diamond (blue curve).

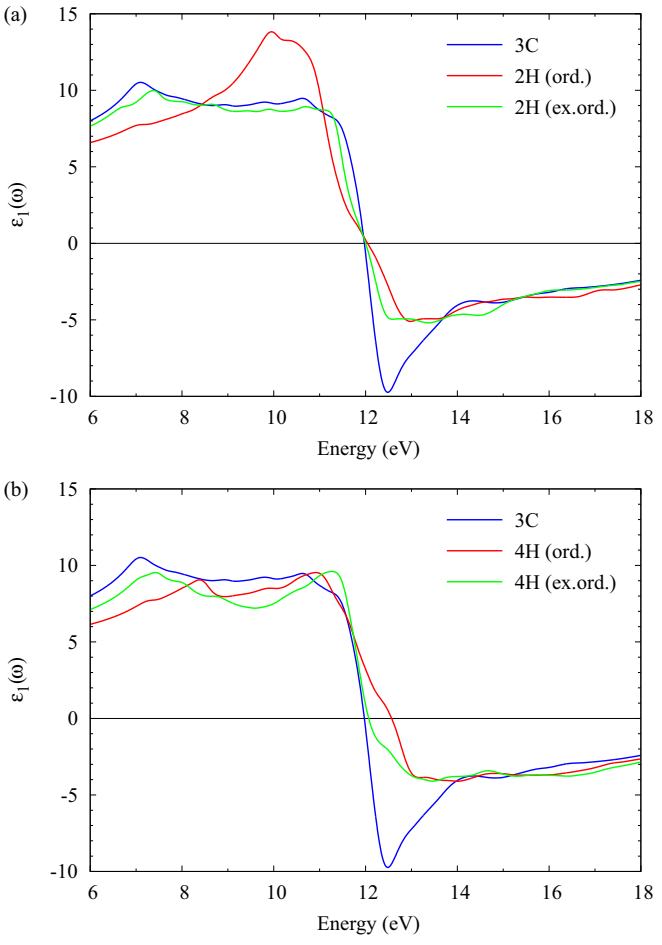

FIG. 5. Real part of the dielectric function $\varepsilon_1(\omega)$ of cubic ($3C$) diamond (blue curve) is compared to those of (a) hexagonal ($2H$) diamond and (b) $4H$ diamond, respectively. The red (green) curve denotes the ordinary (extraordinary) spectra calculated for the polarization of light perpendicular (parallel) to the c axis.

$2H$ and $4H$ diamond, obtained with the BSE method, is shown in Figs. 4(a) and 4(b), respectively, where the BSE spectrum of cubic diamond is also plotted for comparison. The extraordinary spectrum of $2H$ diamond is quite similar to that of cubic diamond, except for a peak with reduced weight that occurred at a slightly lower energy (11.6 eV). The ordinary spectrum of $2H$ diamond has much less weight at low energies before a sharp rise, reaching a absorption maximum at 11.2 eV. The spectrum also exhibits a shoulder around 12.5 eV, which is not seen in the spectrum of cubic diamond at this energy. The extraordinary spectrum of $4H$ diamond exhibits a pronounced peak at 11.8 eV, which is a common feature among the spectra of three diamond polytypes. The ordinary spectrum of $4H$ diamond shows a gradual increase at low energies before it yields broad double peaks (at 11.9 and 12.6 eV) that are similar to the peak and the shoulder in the ordinary spectrum of $2H$ diamond. Above 14 eV, the ordinary and extraordinary spectra of $4H$ diamond are practically identical.

From the calculated imaginary part of the dielectric function $\varepsilon_2(\omega)$, we carry out the Kramers-Kronig transformation to obtain the corresponding real part $\varepsilon_1(\omega)$, which is shown in Fig. 5. As in the case of SiC polytypes [12], the ordinary spectra of $2H$ and $4H$ diamond polytypes resemble the ε_1 spectrum of the cubic ($3C$) diamond, except that the ordinary spectra between 12 and 14 eV are suppressed in comparison to that of cubic diamond. In hexagonal ($2H$) diamond, the extraordinary spectrum exhibits a pronounced maximum at 9.9 eV. In the extraordinary spectrum of $4H$ diamond, the first maximum is shifted to a higher energy. Above 14 eV, the ordinary and extraordinary spectra are nearly identical and are also similar to the ε_1 spectrum of cubic diamond. Finally, we obtain the high-frequency dielectric constants for $2H$ and $4H$ diamond polytypes within the BSE method: $\varepsilon_\infty^\perp = 5.02$ and $\varepsilon_\infty^\parallel = 5.38$ for $2H$ diamond, and $\varepsilon_\infty^\perp = 4.66$ and $\varepsilon_\infty^\parallel = 5.11$ for $4H$ diamond. Here, $\varepsilon_\infty^\perp$ ($\varepsilon_\infty^\parallel$) denotes the dielectric constant for the electric field perpendicular (parallel) to the c axis. The obtained values are distinct from each other, helpful for characterization.

IV. SUMMARY

We have studied the quasiparticle energies and the optical properties of diamond polytypes using the *ab initio* many-body

Green's function approach. By performing quasiparticle calculations within the GWA, we have shown that the fundamental gap values of hexagonal ($2H$) and $4H$ diamond polytypes are significantly different from that of cubic diamond as well as that of bct C_4 phase. We have examined the dielectric functions of three diamond polytypes [cubic ($3C$), $2H$, and $4H$] based on the GW plus BSE methodology. The calculated spectra for cubic diamond are in good agreement with experiment, and the spectra calculated for $2H$ and $4H$ diamond polytypes are found to be distinct from that of cubic diamond. We have also suggested that these diamond polytypes are promising materials to fabricate diamond superlattices. Small lattice-constant mismatches are favorable to superlattice structure formation. The sizable band-gap difference, shown in the present GW results, is more suitable for electron confinement than the one realized in the isotope-controlled system.

ACKNOWLEDGMENTS

The authors thank Dr. J. Deslippe (National Energy Research Scientific Computing Center) for helpful discussions on GW and GW plus BSE calculations using the BERKELEYGW code. M.S. and S.S. acknowledge support from the *Nanoscience and Quantum Physics* project through the Global Center of Excellence Program by Ministry of Education, Culture, Sports, Science and Technology (MEXT), Japan. S.S. acknowledges support from Elements Strategy Initiative to Form Core Research Center (MEXT, Japan) through Tokodai Institute for Element Strategy, and JSPS KAKENHI Grant No. JP25107005. Work by S.G.L. was supported by the Center for Computational Study of Excited-State Phenomena in Energy Materials (C2SEPEM) at the Lawrence Berkeley National Laboratory, which is funded by the U.S. Department of Energy, Office of Science, Basic Energy Sciences, Materials Sciences and Engineering Division under Contract No. DE-AC02-05CH11231, as part of the Computational Materials Sciences Program; work by M.S. and J.R.C. was supported by the same under a subcontract. Computational resources were provided by Global Scientific Information and Computing Center (GSIC) at Tokyo Institute of Technology, the Supercomputer Center at the Institute for Solid State Physics, the University of Tokyo, and the Texas Advanced Computing Center (TACC).

[1] *Properties of Silicon Carbide*, edited by G. L. Harris (INSPEC, Institution of Electrical Engineers, London, 1995).
[2] R. E. Hanneman, H. M. Strong, and F. P. Bundy, Science **155**, 995 (1967).
[3] F. P. Bundy and J. S. Kasper, J. Chem. Phys. **46**, 3437 (1967).
[4] T. Yagi, W. Utsumi, M. A. Yamakata, T. Kikegawa, and O. Shimomura, Phys. Rev. B **46**, 6031 (1992).
[5] H. Hirai, K. Kondo, N. Yoshizawa, and M. Shiraishi, Appl. Phys. Lett. **64**, 1797 (1994).
[6] H. Hirai, Y. Tabira, K. Kondo, T. Oikawa, and N. Ishizawa, Phys. Rev. B **52**, 6162 (1995).
[7] Y. Omata, Y. Yamagami, K. Tadano, T. Miyake, and S. Saito, Physica E **29**, 454 (2005).
[8] M. Sakurai and S. Saito, Jpn. J. Appl. Phys. **49**, 02BB05 (2010).
[9] M. Sakurai, Ph.D. thesis, Tokyo Institute of Technology, 2011.
[10] K. Umemoto, R. M. Wentzcovitch, S. Saito, and T. Miyake, Phys. Rev. Lett. **104**, 125504 (2010).
[11] K. Kobayashi and S. Komatsu, J. Phys. Soc. Jpn. **81**, 024714 (2012).
[12] M. Rohlfing and J. Pollmann, Phys. Rev. B **63**, 125201 (2001).
[13] L. Hedin and S. Lundqvist, in *Solid State Physics*, edited by F. Seitz, D. Turnbull, and H. Ehrenreich (Academic, New York, 1969), Vol. 23.
[14] M. S. Hybertsen and S. G. Louie, Phys. Rev. Lett. **55**, 1418 (1985).
[15] M. S. Hybertsen and S. G. Louie, Phys. Rev. B **34**, 5390 (1986).
[16] M. Rohlfing and S. G. Louie, Phys. Rev. B **62**, 4927 (2000).
[17] P. Hohenberg and W. Kohn, Phys. Rev. **136**, B864 (1964).
[18] W. Kohn and L. Sham, Phys. Rev. **140**, A1133 (1965).
[19] P. Giannozzi, S. Baroni, N. Bonini, M. Calandra, R. Car, C. Cavazzoni, D. Ceresoli, G. L. Chiarotti, M. Cococcioni, I. Dabo *et al.*, J. Phys.: Condens. Matter **21**, 395502 (2009).
[20] D. M. Ceperley and B. J. Alder, Phys. Rev. Lett. **45**, 566 (1980).
[21] J. P. Perdew and A. Zunger, Phys. Rev. B **23**, 5048 (1981).
[22] N. Troullier and J. L. Martins, Phys. Rev. B **43**, 1993 (1991).
[23] L. Kleinman and D. M. Bylander, Phys. Rev. Lett. **48**, 1425 (1982).
[24] J. Deslippe, G. Samsonidze, D. A. Strubbe, M. Jain, M. L. Cohen, and S. G. Louie, Comput. Phys. Commun. **183**, 1269 (2012).
[25] See, for example, S. G. Louie, in *Topics in Computational Materials Science*, edited by C. Y. Fong (World Scientific, Singapore, 1997).
[26] M. Rohlfing and S. G. Louie, Phys. Rev. Lett. **81**, 2312 (1998).
[27] J. Deslippe, G. Samsonidze, M. Jain, M. L. Cohen, and S. G. Louie, Phys. Rev. B **87**, 165124 (2013).
[28] S. Fahy and S. G. Louie, Phys. Rev. B **36**, 3373 (1987).
[29] C.-Y. Yeh, Z. W. Lu, S. Froyen, and A. Zunger, Phys. Rev. B **46**, 10086 (1992).
[30] C. Raffy, J. Furthmüller, and F. Bechstedt, Phys. Rev. B **66**, 075201 (2002).
[31] A. K. Sharma, H. G. Salunke, G. P. Das, P. Ayyub, and M. S. Multani, J. Phys.: Condens. Matter **8**, 5801 (1996).
[32] Y. I. Matsushita, S. Furuya, and A. Oshiyama, Phys. Rev. Lett. **108**, 246404 (2012).
[33] M. Posternak, A. Baldereschi, A. J. Freeman, E. Wimmer, and M. Weinert, Phys. Rev. Lett. **50**, 761 (1983).
[34] M. Posternak, A. Baldereschi, A. J. Freeman, and E. Wimmer, Phys. Rev. Lett. **52**, 863 (1984).
[35] Y. Miyamoto, A. Rubio, X. Blase, M. L. Cohen, and S. G. Louie, Phys. Rev. Lett. **74**, 2993 (1995).
[36] S. Okada, A. Oshiyama, and S. Saito, Phys. Rev. B **62**, 7634 (2000).
[37] T. Miyake and S. Saito, Phys. Rev. B **68**, 155424 (2003).
[38] R. A. Roberts and W. C. Walker, Phys. Rev. **161**, 730 (1967).
[39] H. Watanabe, C. E. Nebel, and S. Shikata, Science **324**, 1425 (2009).

[40] Manuel Cardona and M. L. W. Thewalt, Rev. Mod. Phys. **77**, 1173 (2005).

[41] F. Giustino, S. G. Louie, and M. L. Cohen, Phys. Rev. Lett. **105**, 265501 (2010).

[42] L. X. Benedict, E. L. Shirley, and R. B. Bohn, Phys. Rev. B **57**, R9385(R) (1998).

[43] S. Sharma, J. K. Dewhurst, A. Sanna, and E. K. U. Gross, Phys. Rev. Lett. **107**, 186401 (2011).

[44] *The Properties of Natural and Synthetic Diamond*, edited by J. E. Field (Academic, London 1992).

[45] D. Edwards and H. Philipp, in *Handbook of Optical Constants of Solids*, edited by E. D. Palik (Academic, Orlando, FL, 1985).